Coupled Axisymmetric Finite Element Model of a Magneto-hydraulic Actuator for Active Engine Mounts

Suryarghya Chakrabarti, Marcelo J. Dapino

Department of Mechanical and Aerospace Engineering,
The Ohio State University, Columbus, OH, USA, 43210

ABSTRACT

A coupled axisymmetric finite element model is formulated to describe the dynamic performance of a hydraulically amplified Terfenol-D mount actuator. The formulation is based on the weak form representations of Maxwell's equations for electromagnetics and Navier's equation for mechanical systems. Terfenol-D constitutive behavior is modeled using a fully coupled energy averaged model. Fluid pressure is computed from the volumetric deformation of the fluid chamber and coupled back to the structure as tractions on the boundaries encompassing the fluid. Seal friction is modeled using the Lugre friction model. The resulting model equations are coded into COMSOL (a commercial finite element package) which is used for meshing and global assembly of matrices. Results show that the model accurately describes the mechanical and electrical response of the actuator under static and dynamic conditions. At higher frequencies there are some errors in the phase due to the anhysteretic nature of the Terfenol-D constitutive law. A parametric study reveals that the performance of the actuator can be significantly improved by stiffening the fluid chamber components and reducing seal friction.

Keywords: Terfenol-D, engine mount, hydraulic amplification, magnetostriction, axisymmetric finite element

1. INTRODUCTION

Magnetostrictive materials deform in response to applied magnetic fields and change their magnetization state when stressed. These processes come about by inherent moment realignments which have extremely small response times making these materials suitable for high frequency actuation and sensing mechanisms. One such application is in active powertrain mounts which require a broadband actuator to actively control the pressure of the hydraulic fluid in the mount so as to reduce its dynamic stiffness. To achieve the high stroke requirement of an engine mount actuator ($\approx$ 2 mm), implementation of smart material drivers capable of broadband response requires stroke amplification. Hydraulic amplification[1,2] is particularly attractive as it provides large mechanical gains in a restricted space. Ushijima and Kumakawa[3] developed a piezo-hydraulic actuator with a stroke of 70 μm which uses the hydraulic fluid in the mount for amplification. Shibayama et al.[4] developed a hydraulically amplified piezo actuator in which the hydraulic fluid used for amplification was separately sealed from the fluid in the mount. Chakrabarti and Dapino[5] combined a conventional magnetostrictive Terfenol-D driver with a hydraulic amplification mechanism to obtain millimeter stroke with a bandwidth of over 200 Hz. Due to the presence of material nonlinearities, internal friction, and fluid chamber compliances, linear models considering 100 % energy transmission greatly overestimate the performance of such actuators.[1,6] Chakrabarti and Dapino[7] developed a lumped parameter model considering seal friction, nonlinear Terfenol-D material response and compliance of the fluid chamber components to model the behavior of their magneto-hydraulic actuator. Although the model can accurately quantify the dynamic mechanical response of their actuator, it is not suitable for transducer design because parameters such as fluid chamber compliance and current-field relationships are difficult to quantify in lumped parameter models. A finite element model is more appropriate for design optimization as it can describe effects of both geometry and material constitutive parameters (Young's modulus, permeability, and electrical conductivity) on the dynamic performance of the transducer.

Further author information: (Send correspondence to M.J.D)
S.C.: E-mail: chakrabarti.3@osu.edu, Telephone: 1-614-247-7480
M.J.D.: E-mail: dapino.1@osu.edu, Telephone: 1-614-688-3689

Industrial and Commercial Applications of Smart Structures Technologies 2011,
Edited by Kevin M. Farinholt, Steve F. Griffin, Proc. of SPIE Vol. 7979, 79790C
 · doi: 10.1117/12.881158

Significant research effort has been concentrated on developing an efficient finite element scheme for magnetostrictive transducers. Benbouzid[8] formulated a 2D bidirectionally coupled magnetostatic model with Terfenol-D constitutive behavior modeled using surface splines. Kannan and Dasgupta[9] formulated a 2D magnetostatic model with bi-directionally coupled magnetomechanical relations, current induced magnetic fields and electromagnetic body forces. Zhou et al.[10] developed a 2D dynamic finite element model of a unimorph actuator with one way magnetomechanical coupling. The one way coupled 3D model of Kim and Jung[11] describes force due to magnetostriction driving a coupled fluid-structural model for a sonar transducer. Evans and Dapino[12] presented a fully coupled dynamic model for 3D magnetostrictive transducers simultaneously including the effects of eddy currents, structural dynamics, and flux leakage on transducer performance.

The present work aims at coupling the weak form equations by Evans et al.[12] with a nonlinear energy averaged model for Terfenol-D to describe the response of the magneto-hydraulic mount actuator developed by Chakrabarti and Dapino.[5] In order to exploit the axisymmetric geometry of the device, the equations are reduced to a 2D axisymmetric form. Vector magnetic potential $\mathbf{A}$ and current density $\mathbf{J}$ are reduced to scalars defined in the out-of-plane direction. Fluid pressure in the actuator is computed as a product of the volumetric change of the fluid chamber and the bulk modulus of the fluid. The computed pressure is coupled to the structural model through traction terms on the edges exposed to the fluid. Friction at the o-ring seals is described using the LuGre friction model which describes friction as an interaction force between microscopic bristles present on the sliding surfaces in contact. The complete system of equations is coded into COMSOL (a commercial finite element package) using the weak form mode. COMSOL is used for geometric modeling, meshing and global assembly of matrices. Section 3 describes the formulation in detail while section 4 discusses the constitutive law for Terfenol-D used in this work. Section 5 describes the time-integration scheme used to solve the nonlinear coupled system. This is followed by comparison of modeled responses to measurements along with a parametric study highlighting the sensitivity of the dynamic performance of the actuator to different design parameters in section 6.

2. MAGNETO-HYDRAULIC ACTUATOR (MHA)

Figure 1 shows the geometry of the modeled device. The MHA has a fluid chamber with a large diameter piston at one end driven by a Terfenol-D rod and a small diameter driven piston at the other end. The magnetic circuit

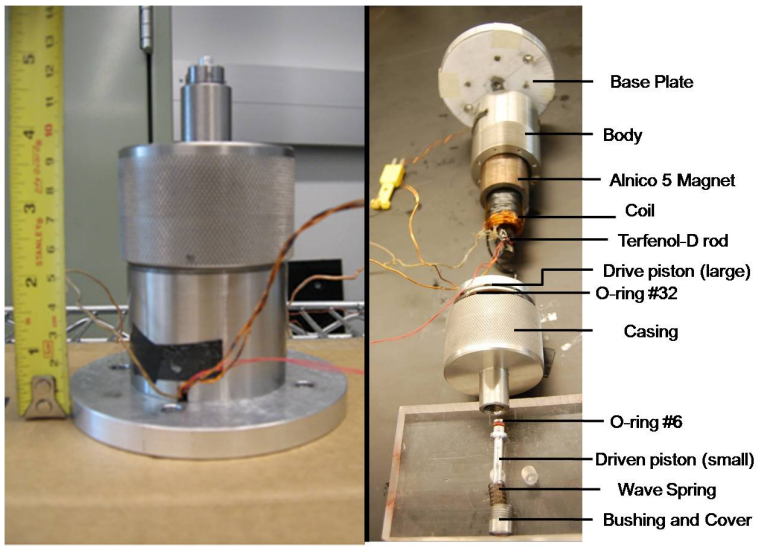

Figure 1. Assembled and exploded view of the Magneto-Hydraulic Actuator.

consists of a permanent magnet to provide magnetic bias, a coil to generate the dynamic fields with Terfenol-D at its core, and iron pieces for flux return. Figure 2 shows the 2D axisymmetric version used for modeling. Some components like the stainless steel body and the preload plate have not been modeled as they serve only a geometrical purpose. The device is surrounded by air so that the magnetic potential boundary condition can be applied to the outer boundary of air. In general, flux density measurements are taken by winding a pick-up coil around the middle of the rod and strain measurements are taken by bonding a strain gage close to the midpoint of the rod. Breaking the magnetostrictive rod domain into 3 areas allows us to evaluate the variables in the central region separately and compare the behavior of the model against measurements. In this actuator, the base plate, Terfenol-D rod, end caps, pistons, and casing are considered to be structurally active. Of these, the end caps, Terfenol-D, and the smaller piston are considered to be only axially active (meaning radial displacement is assumed to be zero) while the others are both radially and axially active.

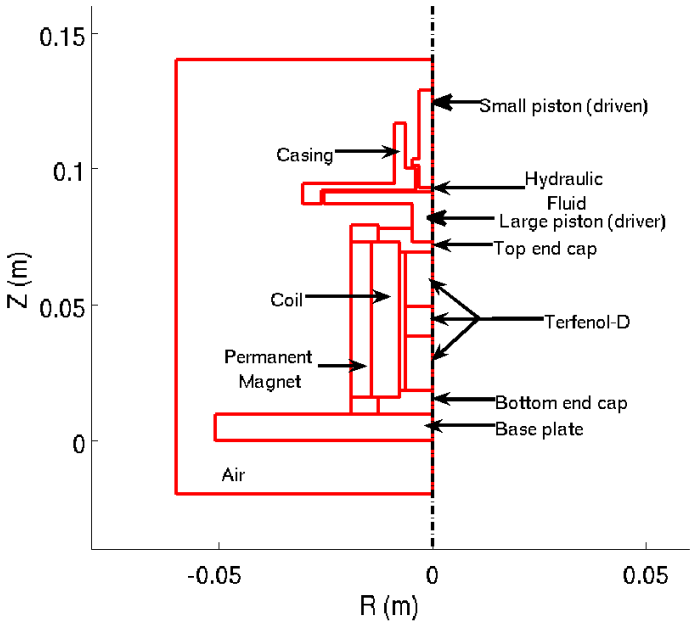

Figure 2. Geometry of the transducer used in this study.

3. MODEL FORMULATION

Global relationships and weak form equations

A large number of magnetostrictive transducers are axisymmetric in nature with the magnetostrictive driver at the core surrounded by a concentric drive coil, permanent magnets, and flux return components. The axisymmetric formulation for electromagnetic problems is an extremely useful tool to efficiently model such transducers without sacrificing accuracy. The current density $\mathbf{J}$ and magnetic potential $\mathbf{A}$ are defined as having only an out-of-plane component (J_ϕ and A_ϕ written as J and A respectively for convenience). Therefore, the magnetic flux density $\mathbf{B}$ has a radial and axial component only, given by

$$B_r = -\frac{\partial A}{\partial z}, \qquad B_z = \frac{1}{r}\frac{\partial}{\partial r}(rA). \tag{1}$$

To avoid singularity in the calculation of B_z at $r = 0$, the variable used in this formulation is $A' = A/r$. With this definition B_r and B_z are given by

$$B_r = -r\frac{\partial A'}{\partial z}, \qquad B_z = r\frac{\partial A'}{\partial r} + 2A'. \tag{2}$$

Similarly, the strain vector is given by four components which are related to the modified radial displacement $u' = u/r$ and axial displacement w as

$$\boldsymbol{\epsilon} = [\epsilon_r, \epsilon_z, \gamma_{rz}, \epsilon_\phi]^{\mathrm{T}} = \left[r\frac{\partial u'}{\partial r} + u', \frac{\partial w}{\partial z}, r\frac{\partial u'}{\partial z} + \frac{\partial w}{\partial r}, u' \right]^{\mathrm{T}}. \tag{3}$$

Although the solution variables are A', u', and w, the weak form equations can be entered in COMSOL as a function of A, u, w, and the corresponding test variables by adding global definitions of A and u in terms of A' and u'.

The weak form equations for a generalized magnetostrictive system can be written as done by Evans et al.[12] as

$$\int_{V_B} \mathbf{H} \cdot \delta\mathbf{B}\ dV + \int_{V_B} \sigma\frac{\partial \mathbf{A}}{\partial t} \cdot \delta\mathbf{A}\ dV = \int_{\partial V_B} \mathbf{H}_T \cdot \delta\mathbf{A}\ d\partial V + \int_{V_B} \mathbf{J}_s \cdot \delta\mathbf{A}\ dV, \tag{4}$$

$$\int_{V_u} \mathbf{T} \cdot \delta\mathbf{S}\ dV + \int_{V_u} \rho\frac{\partial^2 \mathbf{u}}{\partial t^2} \cdot \delta\mathbf{u}\ dV + \int_{V_u} c\frac{\partial \mathbf{u}}{\partial t} \cdot \delta\mathbf{u}\ dV = \int_{\partial V_u} \mathbf{t} \cdot \delta\mathbf{u}\ d\partial V + \int_{V_u} \mathbf{f}_B \cdot \delta\mathbf{u}\ dV. \tag{5}$$

For an axisymmetric problem the volume integrals can be transformed to area integrals using

$$\int_{V_e} (F) dV = 2\pi \int_{A_e} (rF) dr dz. \tag{6}$$

The modified weak form equations can now be written as

$$\int_{A_B} r\mathbf{H} \cdot \delta\mathbf{B}\ dr dz + \int_{A_B} r\sigma\frac{\partial A}{\partial t}\delta A\ dr dz = \int_{l_B} rH_T \delta A\ dl + \int_{A_B} rJ_s \delta A\ dr dz, \tag{7}$$

$$\int_{A_u} r\left(\mathbf{T} \cdot \delta\mathbf{S}\right)\ dr dz + \int_{A_u} r\rho\frac{\partial^2 \mathbf{u}}{\partial t^2} \cdot \delta\mathbf{u}\ dr dz + \int_{A_u} rc\frac{\partial \mathbf{u}}{\partial t} \cdot \delta\mathbf{u}\ dV = \int_{l_u} r\mathbf{t} \cdot \delta\mathbf{u}\ dl + \int_{A_u} r\mathbf{f}_B \cdot \delta\mathbf{u}\ dA. \tag{8}$$

where the vectors $\mathbf{H}$, $\mathbf{B}$, $\mathbf{T}$, $\mathbf{S}$, $\mathbf{u}$ are

$$\begin{aligned} &\mathbf{B} = \begin{bmatrix} B_r & B_z \end{bmatrix}^{\mathrm{T}}, \quad \mathbf{H} = \begin{bmatrix} H_r & H_z \end{bmatrix}^{\mathrm{T}}, \quad \mathbf{u} = \begin{bmatrix} u & w \end{bmatrix}^{\mathrm{T}}, \\ &\mathbf{S} = \begin{bmatrix} S_{rr} & S_{zz} & S_{\phi\phi} & S_{rz} \end{bmatrix}^{\mathrm{T}}, \quad \mathbf{T} = \begin{bmatrix} T_{rr} & T_{zz} & T_{\phi\phi} & T_{rz} \end{bmatrix}^{\mathrm{T}}. \end{aligned} \tag{9}$$

In case of Terfenol loaded axially, the relationship can be simplified by assuming that radial deformation of the rod is negligible. Thus, the strain and stress vectors are reduced to two components (axial and in plane shear).

Fluid Domain

The fluid domain is modeled as having only a capacitive component. The change in volume of the fluid domain ΔV_f can be written as a sum of contributions from the driver piston ΔV_P, the driven piston ΔV_L, and the casing ΔV_C as

$$\Delta V_f = -\Delta V_P + \Delta V_L + \Delta V_C, \tag{10}$$

where each of these volume changes are calculated using the integral

$$\Delta V_i = \int_{l_i} 2\pi r w dr, \tag{11}$$

over the length of the edge l_i exposed to the fluid domain. These can be added in COMSOL as boundary integration variables. The pressure change in the fluid is

$$\Delta p = -\frac{\beta}{V_{ref}} \Delta V_f. \tag{12}$$

The fluid pressure is coupled to the structural model through traction on the edges exposed to the fluid. The model describes the effect of the compliance of fluid chamber components. Here, β is the effective bulk modulus of the fluid alone, while in the lumped parameter model,[7] β_{eff} represented an effective modulus describing the combined compliance of the fluid and fluid chamber components.

Friction model

Friction forces are present at the o-ring seals on the two pistons. Friction at the small driven piston seal has a significant impact on the dynamic response of the actuator since actuation forces are low and velocities are high at this end. On the other hand at the large driver piston end, actuation forces are high and velocities are low; hence a small frictional force at this end does not affect the dynamic response of the actuator. Thus, friction has been modeled only at the smaller piston seal.

In the LuGre model,[13] friction between two sliding surfaces in contact is described as an interaction force between microscopic bristles on both surfaces. The bristle deflection state Z_L is governed by a nonlinear first order differential equation;

$$\dot{Z}_L + \sigma_0 \frac{|v_L|}{g(v_L)} Z_L - v_L = 0, \tag{13}$$

where v_L is the relative sliding velocity between the two surfaces, which in this case is the average velocity of the driven piston calculated by integrating $2\pi r\dot{w}$ over the edge of the piston adjacent to the casing, divided by the area of that surface. Function $g(v_L)$ is given by

$$g(v_L) = F_c + (F_s - F_c)e^{-(v_L/v_s)^2}, \tag{14}$$

where F_s and F_c are the static and Coulomb friction forces and v_s is the Stribeck velocity. The friction force is given by

$$FR_L = \sigma_0 Z_L + \sigma_1 \dot{Z}_L + \sigma_2 v_L, \tag{15}$$

where σ_0 and σ_1 are the bristle stiffness and bristle damping coefficient, respectively. This force is applied as traction on the boundary of the smaller piston adjacent to the casing.

Boundary Conditions

Boundary conditions for an axisymmetric problem must be implemented carefully such that none of the variables become infinite at the $r = 0$ boundary. In this case, the axial symmetry condition is enforced using $(\partial A/\partial r)_{(r=0)} = 0$ in the magnetically active domains, $u_{(r=0)} = 0$ in the radially active domains, and $(\partial w/\partial r)_{(r=0)} = 0$ in the axially active domains. These conditions remove shear stresses and constrain the radial displacement at the $r = 0$ boundary. The magnetostrictive system is encapsulated by a large volume of air. At the outer boundaries of this air volume, the magnetic potential is set to zero. The bottom face of the base plate and the casing are considered to be mechanically fixed.

4. CONSTITUTIVE LAWS

Terfenol-D Constitutive Model

Modeling the constitutive behavior of Terfenol-D has been a traditionally difficult problem. The presence of a large magnetostriction anisotropy, low magnetocrystalline anisotropy, and a twinned dendritic structure gives rise to complex domain level processes which are not completely understood.[14] The Jiles-Atherton model[15] has been commonly used to model actuators based on Terfenol-D loaded unidirectionally,[16,17] but detailed material characterization using this model is not available in the literature. Another approach to modeling Terfenol-D was formulated by Armstrong et al.[18] where bulk properties are derived from an expected value of a large number of moments. The model was later extended to include magnetomechanical hysteresis and its efficiency was improved by restricting the choice of moment orientations to the easy magnetization axes[19] (8 $\langle 111 \rangle$ directions for Terfenol-D). Evans and Dapino[20] developed a constitutive model for Galfenol by choosing orientations which minimize a locally defined energy functional about each easy axis direction. This eliminated the loss in accuracy in the Armstrong model due to the restricted choice of moment orientations, and greatly improved computational speed. The total free energy of a domain close to the k^{th} easy axis $\mathbf{c}^k$ is formulated as the sum of local anisotropy energy G_A^k, magnetomechanical coupling energy G_C^k and the Zeeman energy G_Z^k

$$G^k = \underbrace{\frac{1}{2}K^k \|\mathbf{m}^k - \mathbf{c}^k\|^2}_{G_A^k} \underbrace{- \mathbf{S}_m^k \cdot \mathbf{T}}_{G_C^k} \underbrace{- \mu_0 M_s \mathbf{m}^k \cdot \mathbf{H}}_{G_Z^k}. \tag{16}$$

Minimization of the energy functional and linearization of unity norm constraint on the orientation vectors ($\mathbf{m}^k \cdot \mathbf{m}^k = 1 \approx \mathbf{c}^k \cdot \mathbf{m}^k = 1$) yields the following expression for the k^{th} local minimum

$$\mathbf{m}^k = \left(\mathbf{K}^k\right)^{-1} \left[\mathbf{B}^k + \frac{1 - \mathbf{c}^k \cdot \left(\mathbf{K}^k\right)^{-1} \mathbf{B}^k}{\mathbf{c}^k \cdot \left(\mathbf{K}^k\right)^{-1} \mathbf{c}^k} \mathbf{c}^k\right], \tag{17}$$

where the magnetic stiffness matrix $\mathbf{K}^k$ and force vector $\mathbf{B}^k$ are

$$\mathbf{K}^k = \begin{bmatrix} K^k - 3\lambda_{100}T_1 & -3\lambda_{111}T_4 & -3\lambda_{111}T_6 \\ -3\lambda_{111}T_4 & K^k - 3\lambda_{100}T_2 & -3\lambda_{111}T_5 \\ -3\lambda_{111}T_6 & -3\lambda_{111}T_5 & K^k - 3\lambda_{100}T_3 \end{bmatrix}, \tag{18}$$

$$\mathbf{B}^k = \begin{bmatrix} c_1^k K^k + \mu_0 M_s H_1 & c_2^k K^k + \mu_0 M_s H_2 & c_3^k K^k + \mu_0 M_s H_2 \end{bmatrix}^{\mathrm{T}}. \tag{19}$$

The anhysteretic volume fractions are calculated explicitly using Boltzmann-type averaging,

$$\xi_{an}^k = \frac{\exp\left(-G^k/\Omega\right)}{\sum_{j=1}^{r} \exp\left(-G^j/\Omega\right)}, \tag{20}$$

where Ω is a constant averaging factor.

This energy averaged model has two major shortcomings when applied to Terfenol-D. First, there is an extra kink in the modeled response and secondly, the experimentally observed slow approach to saturation is absent. Assuming a [112] oriented sample, the intermediate kinks occur when domains align along the easy axes oriented 61.9° from the sample axis. Absence of kinks in the measurements suggests that domains are prevented from orienting along these directions. This can be modeled by superimposing an orientation dependent global anisotropy energy on to the local anisotropy energy defined around each easy axis direction as

$$G_A^k = w^k G_{A_0}^k + \frac{1}{2} K^k \|\mathbf{m}^k - \mathbf{c}^k\|^2, \tag{21}$$

where $G_{A_0}^k$ is the global anisotropy energy, which for materials with cubic anisotropy has the form[21]

$$G_{A_0}^k = K_4(m_1^{k^2} m_2^{k^2} + m_2^{k^2} m_3^{k^2} + m_3^{k^2} m_1^{k^2}) + K_6(m_1^{k^2} m_2^{k^2} m_3^{k^2}), \tag{22}$$

weighted by w^k, an empirical weighting factor which adjusts the anisotropy energy along the k^{th} easy axis. The 8 easy axes can be broken down into 3 groups depending upon their angle with the sample axis implying that only three weights need to be determined.

The experimentally observed slow approach to saturation can be obtained by defining the smoothing factor as a function of deviation of anhysteretic domain volume fractions $\boldsymbol{\xi}_{an}$ from a homogeneous distribution $\bar{\boldsymbol{\xi}}$ as

$$\Omega = a_0 + a_1 \|\boldsymbol{\xi}_{an} - \bar{\boldsymbol{\xi}}\|^2. \tag{23}$$

This new definition of Ω destroys the explicit nature of the model since Ω is defined as a function of $\boldsymbol{\xi}_{an}$ while determination of $\boldsymbol{\xi}_{an}$ requires knowledge of Ω given by (20). The correct values of Ω and ξ_{an}^k are obtained by performing Newton-Raphson iterations. Even with strict tolerances, usually two to three iterations are sufficient for convergence. Figure 3 shows the performance of the model in describing the measurements presented by Moffett et al.[22]

As is common with a vector magnetic-potential-based formulation, the constitutive law needs to be inverted to take flux density and strain tensors as input and calculate stress and field. This inversion is done using the quasi-newton SR1 matrix update formula which updates the Jacobian inverse directly eliminating the need for any matrix inversion within the iteration loop. The computed Jacobian inverse in the final iteration of the inversion process is stored and used by COMSOL for the assembly of the global stiffness matrix.

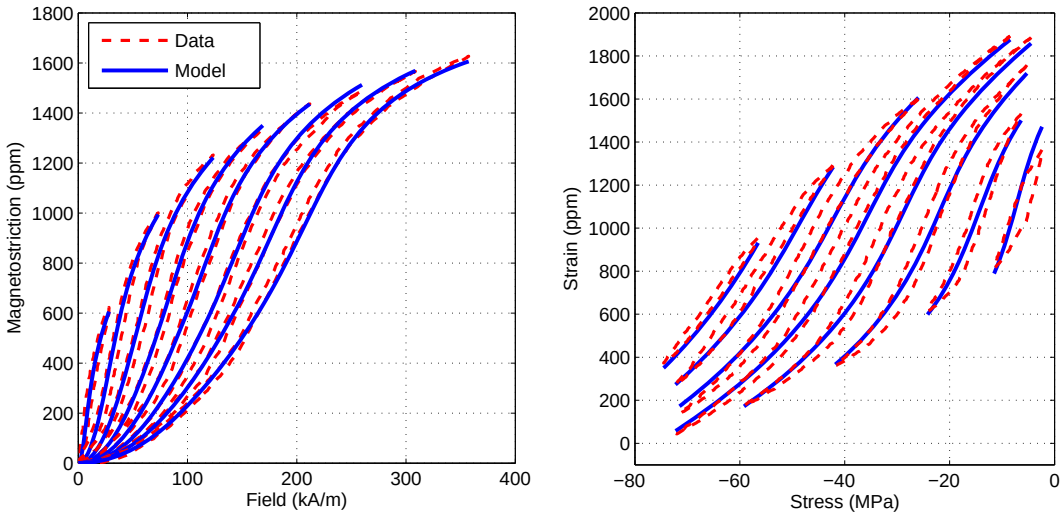

Figure 3. Comparison of the proposed anhysteretic energy averaged model with measurements collected by Moffett et al.[22] All curves have been obtained with the same set of parameters.

Constitutive laws for passive materials

The stress strain laws for passive structural materials (such as steel) can be written as shown by Chandrupatla and Belegundu[23]

$$\begin{Bmatrix} T_{rr} \\ T_{zz} \\ T_{\phi\phi} \\ T_{rz} \end{Bmatrix} = \frac{E(1-\nu)}{(1+\nu)(1-2\nu)} \begin{bmatrix} 1 & \frac{\nu}{(1-\nu)} & \frac{\nu}{(1-\nu)} & 0 \\ \frac{\nu}{(1-\nu)} & 1 & \frac{\nu}{(1-\nu)} & 0 \\ \frac{\nu}{(1-\nu)} & \frac{\nu}{(1-\nu)} & 1 & 0 \\ 0 & 0 & 0 & \frac{(1-2\nu)}{2(1-\nu)} \end{bmatrix} \begin{Bmatrix} S_{rr} \\ S_{zz} \\ S_{\phi\phi} \\ S_{rz} \end{Bmatrix}. \tag{24}$$

The magnetic constitutive laws for passive magnetic materials have been modeled using the linear isotropic relationship $\mathbf{H} = \mu^{-1}\mathbf{B}$ where μ is the constant permeability of the material. For permanent magnets this law is modified to include the residual induction B_{res} in the relevant direction. For example, if the residual induction is along the z direction, the constitutive law can be written as

$$H_r = \frac{1}{\mu} B_r, \tag{25}$$

$$H_z = \frac{1}{\mu} \left(B_z - B_{res} \right). \tag{26}$$

Electrically conducting materials have been modeled using a constant conductivity.

5. NONLINEAR DYNAMIC SOLUTION PROCEDURE

Solution of nonlinear dynamic systems is a particularly challenging task as even unconditionally stable schemes for linear systems may become unstable. In this work an implicit time integration scheme is followed based on the trapezoidal rule as described by Bathe.[24] The governing equations for the coupled finite element system can be written as

$$\mathbf{M}\ddot{\mathbf{U}} + \mathbf{D}\dot{\mathbf{U}} = \mathbf{R}(t) - \mathbf{F}(\mathbf{U}, t), \tag{27}$$

where the mass matrix $\mathbf{M}$, damping matrix $\mathbf{D}$ and state vector $\mathbf{U}$ are of the form

$$\mathbf{M} = \begin{bmatrix} \mathbf{0} & \mathbf{0} \\ \mathbf{0} & \mathbf{M}^u \end{bmatrix}, \quad \mathbf{D} = \begin{bmatrix} \mathbf{D}^A & \mathbf{0} \\ \mathbf{0} & \mathbf{D}^u \end{bmatrix}, \quad \mathbf{U} = \begin{pmatrix} \mathbf{Q}^A \\ \mathbf{Q}^u \end{pmatrix}. \tag{28}$$

The vector of externally applied forces $\mathbf{R}(t)$ includes contributions from the coil source current density, tangential applied fields, point forces, and/or traction on certain boundaries. $\mathbf{F}(\mathbf{U},t)$ is the internal nodal force vector whose derivative with respect to the state vector $\mathbf{U}$ yields the stiffness matrix. Since $\mathbf{F}$ contains contributions from field and stress which are nonlinearly dependent on $\mathbf{U}$, the stiffness matrix $\mathbf{K}$ is also state dependent. Bathe[24] suggested various time-integration schemes for nonlinear structural problems of similar form. Explicit methods are ruled out since the mass matrix is singular. An implicit scheme based on the trapezoidal rule is implemented, combined with equilibrium iterations. At the k^{th} iteration the system equations can be written as

$$\mathbf{M}\ddot{\mathbf{U}}^{(k)} + \mathbf{D}\dot{\mathbf{U}}^{(k)} + {}^{t+\Delta t}\mathbf{K}^{(k-1)}\Delta\mathbf{U}^{(k)} = {}^{t+\Delta t}\mathbf{R} - {}^{t+\Delta t}\mathbf{F}^{(k-1)}, \tag{29}$$

$${}^{t+\Delta t}\mathbf{U}^{(k)} = {}^{t+\Delta t}\mathbf{U}^{(k-1)} + \Delta\mathbf{U}^{(k)}. \tag{30}$$

According to the trapezoidal rule of time integration, the following assumptions are used

$${}^{t+\Delta t}\mathbf{U} = {}^{t}\mathbf{U} + \frac{\Delta t}{2}\left({}^{t}\dot{\mathbf{U}} + {}^{t+\Delta t}\dot{\mathbf{U}}\right), \tag{31}$$

$${}^{t+\Delta t}\dot{\mathbf{U}} = {}^{t}\dot{\mathbf{U}} + \frac{\Delta t}{2}\left({}^{t}\ddot{\mathbf{U}} + {}^{t+\Delta t}\ddot{\mathbf{U}}\right). \tag{32}$$

The vectors $\ddot{\mathbf{U}}^{(k)}$ and $\dot{\mathbf{U}}^{(k)}$ can be written using (30) to (32) as

$${}^{t+\Delta t}\ddot{\mathbf{U}}^{(k)} = \frac{4}{\Delta t^2}\left({}^{t+\Delta t}\mathbf{U}^{(k-1)} - {}^{t}\mathbf{U} + \Delta\mathbf{U}^{(k)}\right) - \frac{4}{\Delta t}{}^{t}\dot{\mathbf{U}} - {}^{t}\ddot{\mathbf{U}}, \tag{33}$$

$${}^{t+\Delta t}\dot{\mathbf{U}}^{(k)} = \frac{2}{\Delta t}\left({}^{t+\Delta t}\mathbf{U}^{(k-1)} - {}^{t}\mathbf{U} + \Delta\mathbf{U}^{(k)}\right) - {}^{t}\dot{\mathbf{U}}. \tag{34}$$

Substitution in (29) yields the equation of motion for the system;

$$\begin{aligned}\left[{}^{t+\Delta t}\mathbf{K}^{(k-1)} + \frac{4\mathbf{M}}{\Delta t^2} + \frac{2\mathbf{D}}{\Delta t}\right]\Delta\mathbf{U}^{(k)} = {}^{t+\Delta t}\mathbf{R} - \mathbf{M}\left[\frac{4}{\Delta t^2}\left({}^{t+\Delta t}\mathbf{U}^{(k-1)} - {}^{t}\mathbf{U}\right) - \frac{4}{\Delta t}{}^{t}\dot{\mathbf{U}} - {}^{t}\ddot{\mathbf{U}}\right] \\ - \mathbf{D}\left[\frac{2}{\Delta t}\left({}^{t+\Delta t}\mathbf{U}^{(k-1)} - {}^{t}\mathbf{U}\right) - {}^{t}\dot{\mathbf{U}}\right] - {}^{t+\Delta t}\mathbf{F}^{(k-1)}.\end{aligned} \tag{35}$$

The starting values for the iterations are obtained from the values obtained in the previous time step.

$${}^{t+\Delta t}\mathbf{F}^{(0)} = {}^{t}\mathbf{F}, \quad {}^{t+\Delta t}\mathbf{U}^{(0)} = {}^{t}\mathbf{U}. \tag{36}$$

The convergence criteria used in this work are based on energy and the norm of the out-of-balance load vector.[24] Mathematically they can be written as

$$\frac{\|{}^{t+\Delta t}\mathbf{R} - {}^{t+\Delta t}\mathbf{F}^{(k-1)} - \mathbf{M}\ {}^{t+\Delta t}\ddot{\mathbf{U}}^{(k-1)} - \mathbf{D}\ {}^{t+\Delta t}\dot{\mathbf{U}}^{(k-1)}\|}{RNORM} \leq RTOL, \tag{37}$$

$$\frac{\Delta\mathbf{U}^{(k)} \cdot \left({}^{t+\Delta t}\mathbf{R} - {}^{t+\Delta t}\mathbf{F}^{(k-1)} - \mathbf{M}\ {}^{t+\Delta t}\ddot{\mathbf{U}}^{(k-1)} - \mathbf{D}\ {}^{t+\Delta t}\dot{\mathbf{U}}^{(k-1)}\right)}{\Delta\mathbf{U}^{(1)} \cdot \left({}^{t+\Delta t}\mathbf{R} - {}^{t}\mathbf{F} - \mathbf{M}\ {}^{t}\ddot{\mathbf{U}} - \mathbf{D}\ {}^{t}\dot{\mathbf{U}}\right)} \leq ETOL. \tag{38}$$

The mass and damping matrix are state-independent and hence are assembled only once for the entire simulation. The internal nodal force vector $\mathbf{F}$ and the tangential stiffness matrix $\mathbf{K}$ are assembled in every iteration as they are state-dependent. Evaluation of $\mathbf{F}$ requires computation of the total stress and field for a given flux density and strain distribution, for which the Terfenol-D constitutive law needs to be inverted. This is done using the Quasi-Newton SR1 formula which updates the Jacobian inverse directly, eliminating the need for matrix inversion within the iteration loop. The computed Jacobian inverse in the final iteration of the inversion process is used for assembly of the global stiffness matrix.

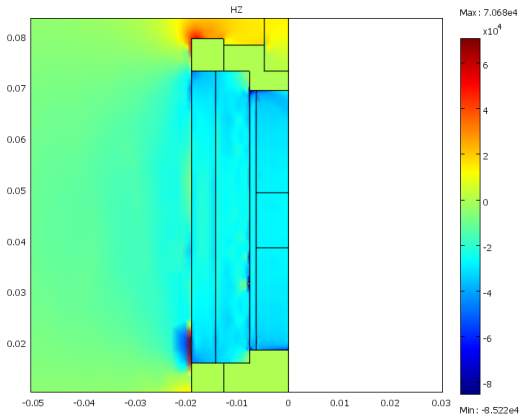

Figure 4. Axial magnetic field distribution in the magnetic circuit due to the permanent magnet.

6. MODEL VALIDATION AND PARAMETRIC STUDY

Obtaining the bias point

To calculate the dynamic response of the actuator, its bias point needs to be accurately determined. The actuator is biased both mechanically and magnetically. The mechanical bias is due to the compression of the wave spring whose force is transmitted (and amplified) through the fluid to the Terfenol-D rod. The stress developed in the Terfenol-D under an axial load can be assumed uniform. Therefore, this stress is superimposed directly on the applied stress in the constitutive model function. The magnetic bias is due to the residual flux density in the permanent magnet. This field depends on the geometry of the magnetic circuit and cannot be assumed to be homogeneously distributed in the rod. The magnetic bias point is obtained by increasing the residual flux density of the magnet from zero to its actual value using a hyperbolic tangent function and storing the solution from the final step. Figure 4 shows that the axial magnetic field at the bias point is uniformly distributed in the central region of the rod with a somewhat lower value at the ends. The average magnetic field in the Terfenol-D rod is ≈ 30 kA/m.

Response to harmonic inputs

Figure 5 shows the actuator response at 20, 50, 100, and 200 Hz. As expected the phase between voltage and displacement increases with increasing frequency resulting in counter-clockwise rotation of the loops. One shortcoming of the model is the assumed anhysteretic Terfenol-D behavior which causes a discrepancy in the phase of the response. At lower frequencies this is not visible but at 200 Hz this difference in phase is prominent. It can be seen in both the experimental and modeled voltage-current loops that the current signal is asymmetric. Although the actuator is driven with an unbiased sinusoidal voltage input, the resulting current signal is biased due to the nonlinear behavior of Terfenol-D. Such effects can only be described with models where electromagnetic and mechanical responses are fully coupled.

Parametric Study

The proposed finite element model can be a useful tool for optimizing device geometry and material selection. To illustrate , the effect of fluid Bulk modulus, Young's modulus of the fluid chamber components, and seal friction force on the unloaded displacement response of the actuator is studied. Since the requirements of a mount actuator are most stringent under engine idling conditions (≈ 20 Hz), the results presented here are obtained by varying parameters for a 20 Hz drive frequency.

The effective fluid bulk modulus usually plays a key role in the dynamic performance of hydraulic devices. In this work, fluid bulk modulus is varied from $0.1\beta_0$ to $2\beta_0$, where β_0 is the manufacturer specified bulk modulus for the fluid. Figure 6(a) shows that even a 50 % reduction in the fluid bulk modulus hardly causes any change in the stroke produced by the actuator. This is because the compliance of the structural fluid chamber components is much higher than that of the fluid itself. A 90 % reduction in the fluid's bulk modulus makes the two compliances

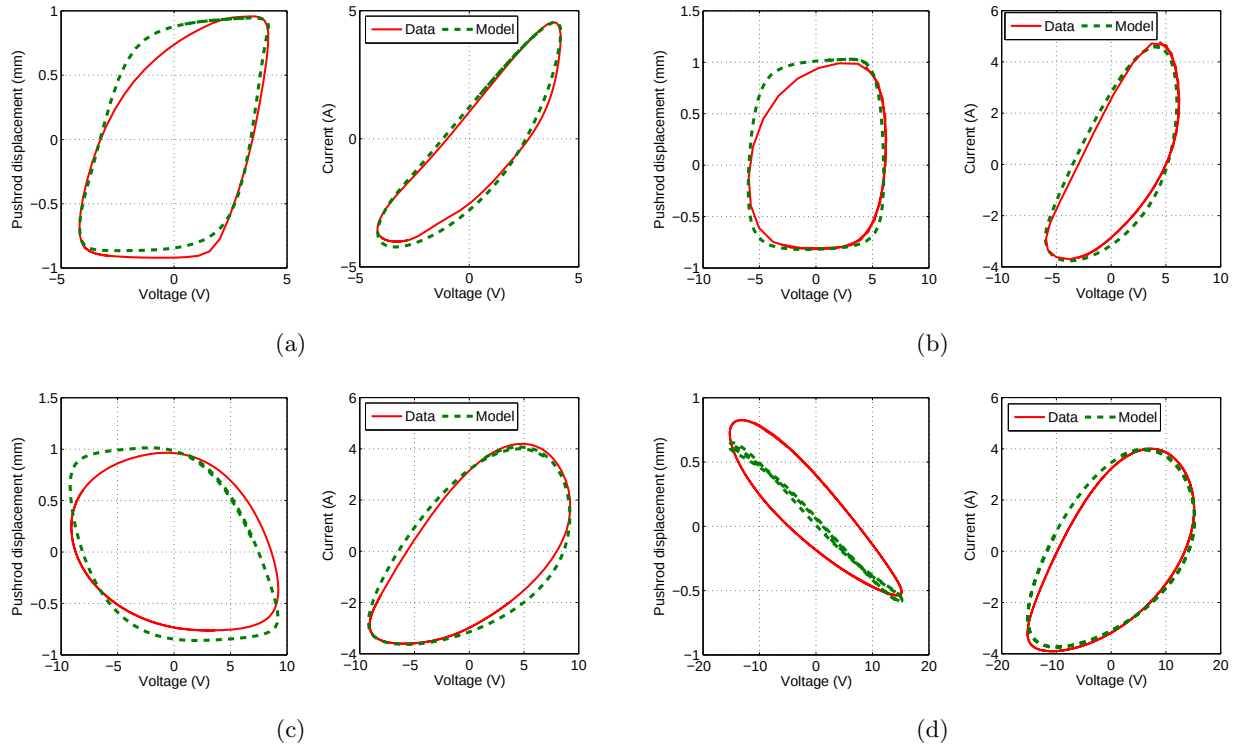

Figure 5. Comparison of modeled voltage-displacement and voltage-current loops with measurements.

closer and a noticeable 20 % drop in the stroke of the actuator is recorded. To illustrate this fact, the Young's modulus of the stainless steel fluid chamber components is increased to 1.5 and 3 times its initial value. The performance of the actuator improves by ≈ 30 % when the Young's modulus is increased 3 times (Figure 6(c)).

Another design parameter which is expected to significantly affect the actuator response is the seal friction force, which is varied by changing the parameters F_c and F_s in (14). Reducing the friction force by half results in a 12 % increase in performance, while removing it completely yields a 24 % increase. Table 1 shows the percentage change in the peak-peak stroke of the actuator for different parameter values. It can be seen that the actuator performance can be significantly enhanced by increasing the stiffness of the fluid chamber components. Further enhancements in performance can be achieved by reducing the friction at the seals. Attempting to increase the effective bulk modulus of the fluid would not have a substantial effect on the actuator's performance. This is primarily due to the extremely low volume of fluid used in this design.

Table 1. Effect of design parameters on the percentage change in the unloaded displacement response of the MHA at 20 Hz (negative sign denotes reduction in performance).

Parameter	% change
$\beta = 0.1\beta_0,\ Es = Es_0,\ Fr = Fr_0$	-20.16
$\beta = 0.5\beta_0,\ Es = Es_0,\ Fr = Fr_0$	-2.40
$\beta = 2\beta_0,\ Es = Es_0,\ Fr = Fr_0$	1.22
$\beta = \beta_0,\ Es = 1.5Es_0,\ Fr = Fr_0$	12.94
$\beta = \beta_0,\ Es = 3Es_0,\ Fr = Fr_0$	31.47
$\beta = \beta_0,\ Es = Es_0,\ Fr = 0.5Fr_0$	11.93
$\beta = \beta_0,\ Es = Es_0,\ Fr = 0.25Fr_0$	18.73
$\beta = \beta_0,\ Es = Es_0,\ Fr = 0$	23.67

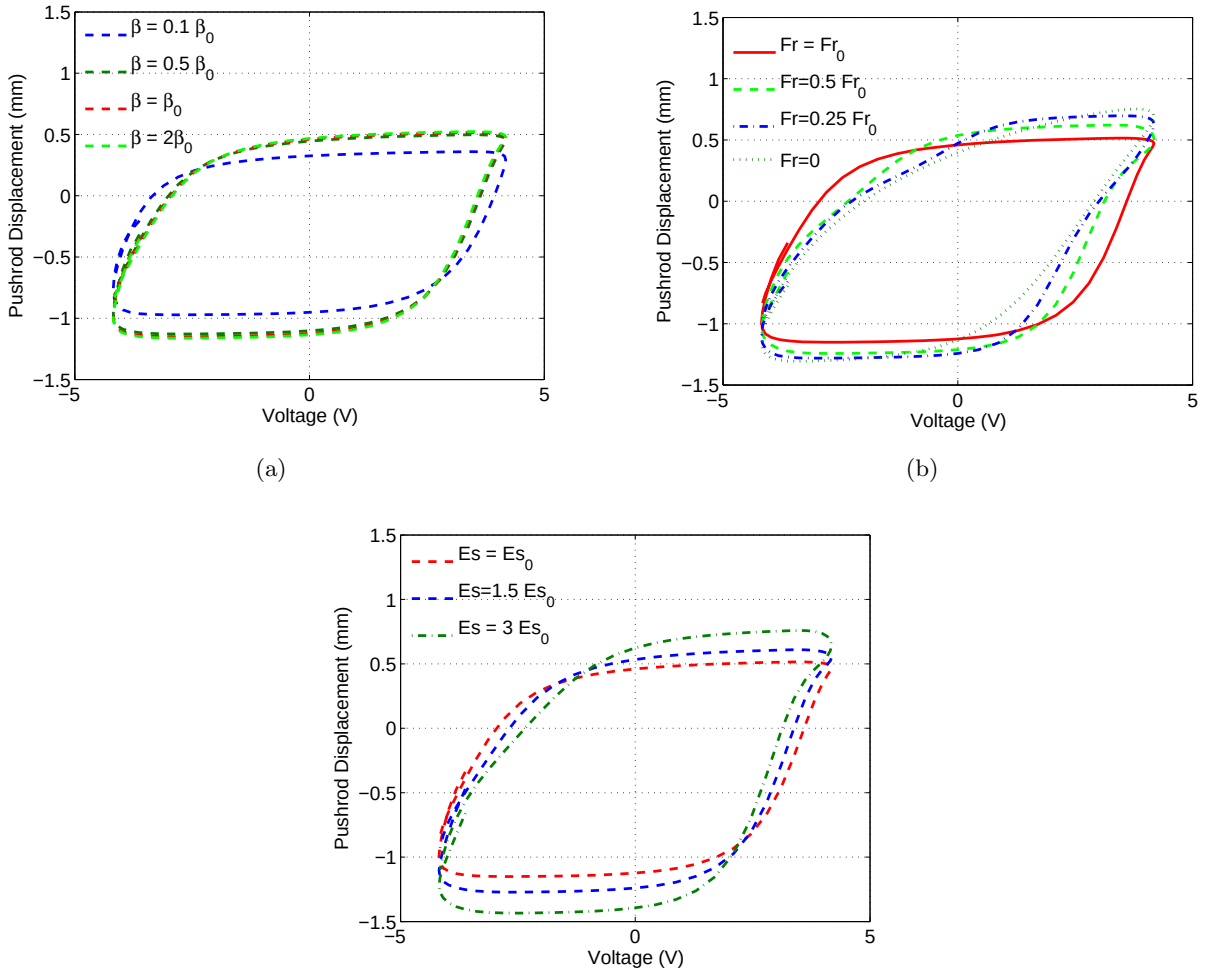

Figure 6. Effect of different design parameters on the unloaded displacement response of the MHA at 20 Hz, (a) Bulk modulus of fluid, (b) Friction forces at the driven pushrod, (c) Young's modulus of fluid chamber components.

7. CONCLUDING REMARKS

This paper presents a coupled axisymmetric finite element model of a Terfenol-D mount actuator. The vector magnetic-potential-based finite element model couples Maxwell's equations and Navier's equations through a nonlinear energy averaged constitutive law for Terfenol-D. The model is capable of describing the dynamic mechanical and electrical behavior of the actuator due to nonlinear Terfenol-D behavior and dynamics of the structure and fluid. At high frequencies the model shows some discrepancy in the phase of the predicted output due to the assumed anhysteretic Terfenol-D constitutive law. A parametric study on the unloaded displacement response of the actuator at 20 Hz (engine idling conditions) shows that increasing the stiffness of the fluid chamber components can substantially improve the actuator's output displacement. Further enhancements in the performance can be made by reducing seal friction. It is also found that the actuator's performance is not very sensitive to changes in bulk modulus of the fluid due to the extremely small fluid volume contained in the hydraulic chamber.

ACKNOWLEDGMENTS

Financial support for this research was provided by the Smart Vehicle Concepts Center, a National Science Foundation Industry/University Collaborative Research Center (www.SmartVehicleCenter.org), and by ONR MURI Grant # N000140610530 (Jan Lindberg program manager).

REFERENCES

[1] Yoon, H.-S., Washington, G., Eyabi, P., Radhamohan, M., Woodard, S. W., and Dayton, R., "A millimeter-stroke piezoelectric hybrid actuator using hydraulic displacement amplification mechanism," *IEEE International Symposium on Industrial Electronics* **4**, 2809–2813 (July 2006).

[2] Giurgiutiu, V., Rogers, C. A., and Rusovici, R., "Solid-State Actuation of Rotor Blade Servo-Flap for Active Vibration Control," *Journal of Intelligent Material Systems and Structures* **7**(2), 192–202 (1996).

[3] Ushijima, T. and Kumakawa, S., "Active engine mount with piezo-actuator for vibration control," *SAE* (930201) (1993).

[4] Shibayama, T., Ito, K., Gami, T., Oku, T., Nakajima, Z., and Ichikawa, A., "Active engine mount for a large amplitude of engine vibration," *SAE* (951298) (1995).

[5] Chakrabarti, S. and Dapino, M., "Design and modeling of a hydraulically amplified magnetostrictive actuator for automotive engine mounts," *Industrial and Commercial Applications of Smart Structures Technologies 2009* **7290**(1), 72900D, SPIE (2009).

[6] Garcia-Bonito, J., Brennan, M. J., Elliott, S. J., David, A., and Pinnington, R. J., "A novel high-displacement piezoelectric actuator for active vibration control," *Smart Materials and Structures* **7**(1), 31–42 (1998).

[7] Chakrabarti, S. and Dapino, M., "A dynamic model for a displacement amplified magnetostrictive driver for active mounts," *Smart Materials and Structures* **19**, 055009 (2010).

[8] Benbouzid, M., Beguenane, R., Reyne, G., and Meunier, G., "Finite element modeling of Terfenol-D magneto-mechanical coupling: application to a direct micro-stepping rotary motor," (1997).

[9] Kannan, K. and Dasgupta, A., "A nonlinear Galerkin finite-element theory for modeling magnetostrictive smart structures," *Smart Materials and Structures* **6**, 341–350 (1997).

[10] Zhou, H. and Zhou, Y., "Vibration suppression of laminated composite beams using actuators of giant magnetostrictive materials," *Smart materials and structures* **16**, 198–206 (2007).

[11] Kim, J. and Jung, E., "Finite element analysis for acoustic characteristics of a magnetostrictive transducer," *Smart Materials and Structures* **14**, 1273–1280 (2005).

[12] Evans, P. and Dapino, M., "Dynamic Model for 3-D Magnetostrictive Transducers," *Magnetics, IEEE Transactions on* **47**(1), 221–230 (2011).

[13] Olsson, H., Astrom, K. J., de Wit, C. C., Gafvert, M., and Lischinsky, P., "Friction models and friction compensation," *Eur. J. Control* **4**(3), 176–195 (1998).

[14] Huang, Y. and Jin, Y., "Phase field modeling of magnetization processes in growth twinned Terfenol-D crystals," *Applied Physics Letters* **93**, 142504 (2008).

[15] Jiles, D. and Atherton, D., "Theory of ferromagnetic hysteresis," *Journal of Magnetism and Magnetic Materials* **61**(1-2), 48 – 60 (1986).

[16] Dapino, M., Smith, R., and Flatau, A., "Structural magnetic strain model for magnetostrictive transducers," *IEEE Transactions on Magnetics* **36**, 545–556 (May 2000).

[17] Huang, W., Wang, B., Cao, S., Sun, Y., Weng, L., and Chen, H., "Dynamic strain model with eddy current effects for giant magnetostrictive transducer," *IEEE Transactions on Magnetics* **43**, 1381–1384 (April 2007).

[18] Armstrong, W., "Magnetization and magnetostriction processes in $tb_0.27 - 0.30dy_0.73 - 0.70fe_1.9 - 2.0$," *Journal of Applied Physics* **81**(5), 23217–2326 (1997).

[19] Armstrong, W. D., "An incremental theory of magneto-elastic hysteresis in pseudo-cubic ferromagnetostrictive alloys," *Journal of Magnetism and Magnetic Materials* **263**, 208 (2003).

[20] Evans, P. G. and Dapino, M. J., "Efficient magnetic hysteresis model for field and stress application in magnetostrictive galfenol," *Journal of Applied Physics* **107**(6), 063906 (2010).

[21] Mei, W., Okane, T., and Umeda, T., "Magnetostriction of Tb–Dy–Fe crystals," *Journal of applied physics* **84**, 6208 (1998).
[22] Moffett, M., Clark, A., Wun-Fogle, M., Linberg, J., Teter, J., and McLaughlin, E., "Characterization of Terfenol-D for magnetostrictive transducers," *The Journal of the Acoustical Society of America* **89**, 1448 (1991).
[23] Chandrupatla, T. and Belegundu, A., [*Introduction to Finite Elements in Engineering*], Prentice-Hall, Upper Saddle River, New Jersey 07458, 3rd ed. (2002).
[24] Bathe, K., [*Finite Element Procedures*], Prentice Hall, Upper Saddle River, New Jersey 07458 (1996).